PNNL-27351

Pacific Northwest NATIONAL LABORATORY

Proudly Operated by Battelle Since 1965

Universal Wide-area Damping Control for Mitigating Inter-area Oscillations in Power Systems

December 2017

Pacific Northwest National Laboratory

J Lian R Huang
S Wang R Fan
MA Elizondo H Kirkham
J Hansen LD Marinovici

Sandia National Laboratories

D Schoenwald F Wilches-Bernal

U.S. DEPARTMENT OF ENERGY

Prepared for the U.S. Department of Energy under Contract DE-AC05-76RL01830

PACIFIC NORTHWEST NATIONAL LABORATORY
operated by
BATTELLE
for the
UNITED STATES DEPARTMENT OF ENERGY
under Contract DE-AC05-76RL01830

Printed in the United States of America

Available to DOE and DOE contractors from the
Office of Scientific and Technical Information,
P.O. Box 62, Oak Ridge, TN 37831-0062;
ph: (865) 576-8401
fax: (865) 576-5728
email: reports@adonis.osti.gov

Available to the public from the National Technical Information Service
5301 Shawnee Rd., Alexandria, VA 22312
ph: (800) 553-NTIS (6847)
email: orders@ntis.gov <http://www.ntis.gov/about/form.aspx>
Online ordering: http://www.ntis.gov

This document was printed on recycled paper.
(8/2010)

PNNL-27351

Universal Wide-area Damping Control for Mitigating Inter-area Oscillations in Power Systems

Pacific Northwest National Laboratory

J Lian	R Huang
S Wang	R Fan
MA Elizondo	H Kirkham
J Hansen	LD Marinovici

Sandia National Laboratories

D Schoenwald	F Wilches-Bernal

December 2017

Prepared for
the U.S. Department of Energy
under Contract DE-AC05-76RL01830

Pacific Northwest National Laboratory
Richland, Washington 99352

Abstract

The active damping of inter-area oscillations of low frequencies has been successfully demonstrated to improve the dynamic response of the power grid in a satisfactory manner. It also enhances the system stability and reliability as well. The existence of inter-area oscillations has already become one of the key challenges in large-scale interconnected power grids because they are detrimental to the achievement of maximum power transfer and optimal power flow. This project focuses on the development of a universal damping control based on phasor measurements so that it can be easily implemented by a mix of various fast-acting resources to effectively mitigate inter-area oscillations. With the proposed advanced damping control strategies, the power grid stability and reliability can be managed in a much more flexible manner by utilizing different resources that are geographically dispersed in both the transmission and distribution systems. Moreover, higher power transfer capacity can be also achieved.

Summary

The occurrence of inter-area oscillations is one of the major threats to the grid stability and reliability in the Western Interconnection of the North American power grid. If not well damped, the ever-growing oscillations can cause the system to break up and then, in the worst case, cause large-scale power outages. There have been several incidents of system-wide oscillations in the U.S. and abroad. The most notable of those incidents is the western system breakup on August 10, 1996, which was caused by undamped system-wide oscillations. During the outage, about 7.5 million customers (involving 24 million people) lost their power supply for periods that lasted from a few minutes to 6 hours. Since then, many efforts have been devoted to the mitigation of system oscillations.

For inter-area oscillation damping, the existing control options in today's power grid include power system stabilizer, supplementary damping controllers associated with flexible alternating current (AC) transmission system (FACTS) devices (e.g., Static Var Compensators), and direct current (DC) line modulation. PSSs have been installed at many generators and have been shown to be effective in damping local oscillations related to local power plants and inter-area oscillations if properly coordinated. The use of DC line modulation has also been demonstrated. Shortly before the Pacific DC Interconnection was commissioned by the Western Electricity Coordinating Council (WECC), it was shown that the appropriate modulation of power flow over the DC line could be effective in damping the north-to-south oscillation mode.[1] However, none these prior efforts on damping the inter-area oscillations in the power grid has been completely successful for the following reasons:

1. Traditional PSSs were designed based on local measurements as feedback signals for parameter tuning. However, local measurements usually contain very little information related to inter-area oscillations, which involve different groups of generators oscillating against each other. Thus, a single PSS that is installed at one generator usually does not "see" these oscillations. In this case, it is not effective for traditional PSSs to damp inter-area oscillations unless careful coordination is achieved among many PSSs that are geographically dispersed.
2. The modulation signals applied to the north-to-south DC line for oscillation damping were derived from the north-to-south power flow in the WECC. Hence, it affected flows into the north and out of the south. However, these changes in power levels could impact areas further afield, and it was reasoned that they might affect those regions unfavorably.
3. For large-scale interconnected power grids, there are usually multiple oscillation modes existing simultaneously. The controller designed for mitigating a specific oscillation mode may adversely affect other modes during the parameter tuning process without proper coordination.

Although active damping for inter-area oscillations in the power grid has been shown to be effective, the anticipated "byproduct" problems must be recognized and dealt with for this technology to be widely applied to the real system. Dealing with these problems by using the phasor measurement unit (PMU) measurements is at the heart of this project. Over the last 20 years, many PMUs have been installed in both the Western and Eastern Interconnections. There were approximately 2000 PMUs altogether in the

[1] Dougherty, J. and T. Hillesland (1970). Power system stability considerations with dynamically responsive DC transmission lines. *IEEE Transactions on Power Apparatus and Systems PAS-89*(1), 34–45.

U.S. by September 2015. The availability of PMU measurements provides better feedback signals for designing more effective controllers for inter-area oscillation damping.

This project will use PMU measurements to develop a universal damping control that can use a mix of various fast-acting resources to effectively mitigate inter-area oscillations in the power grid. Both high voltage DC lines in transmission system and end-use loads in distribution system are explored in this project to implement the proposed universal damping control for inter-area oscillations. Furthermore, a new analytical approach is proposed for decoupled damping control to avoid the adverse interactions among the damping of different oscillation modes. The effectiveness of the proposed control strategies is demonstrated by simulation studies over a reduced-order dynamic model of the WECC system. It can be seen that the power grid stability and reliability can be now managed in a much more flexible manner by utilizing different resources that are geographically dispersed within the grid. Moreover, higher power transfer capacity can be achieved with the improved damping of inter-area oscillations.

Acknowledgments

The authors are grateful to Phil N. Overholt at the U.S. Department of Energy Office of Electricity Delivery and Energy Reliability for supporting this research and development efforts.

Acronyms and Abbreviations

AC	alternating current
DC	direct current
FACTS	flexible AC transmission system
FFT	fast Fourier transform
HVDC	high-voltage DC
IPP	Intermountain Power Project
LCC	line commutated converter
MANGO	Modal Analysis for Grid Operations
PDCI	Pacific DC Intertie
PMU	phasor measurement unit
POD	power oscillation damping
PSS	power system stabilizer
SMIB	single-machine infinite-bus
TWE	TransWest Express transmission project
WAMS	wide-area measurement system
WECC	Western Electricity Coordinating Council

Contents

Figures

Tables

1.0 Introduction

The inter-area oscillations of low frequency are inherent phenomena between synchronous generators that are interconnected by transmission systems. It has been pointed out in (Klein et al. 1991) that these oscillations often become poorly damped with heavy power transfer between different areas over weak connections of long distance. Because sustained oscillations could cause system breakup and even lead to large-scale blackout, it is extremely important to maintain the stability of these oscillations for the system security. However, environmental constraints and economic pressures often push power systems close to their operational limits (Bertsch et al. 2005), which greatly reduces the stability margin of the normal operation. One of the prominent events caused by undamped oscillations is the notable breakup and blackout in the western North American Power System on August 10, 1996 (Kosterev et al. 1999). The measurement of power transfer on Malin-Round Mountain line during that event is shown in Figure 1.

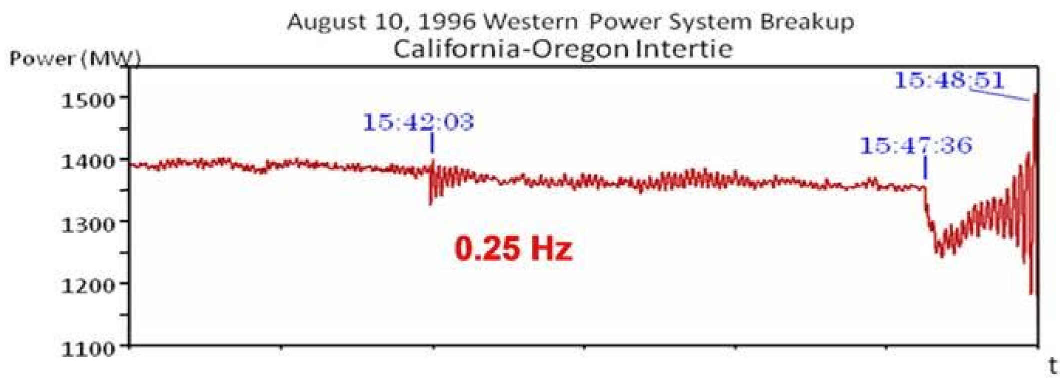

Figure 1. Undamped Oscillations in the Western North American Power System on August 10, 1996

To ensure secure system operation, the amount of power transfer on tie-lines between different areas is often limited due to the inter-area oscillations that are poorly damped. Hence, new control strategies that can improve the damping of these inter-area oscillations are needed to increase the transmission capacity for a better utilization of the existing transmission network. With the growth of power systems interconnections, inter-area mode oscillation has become a serious limiting factor affecting transfer of power in large quantities among different areas.

A well-known damping controller is the power system stabilizer (PSS) (Kundur 1994). It adds a supplementary control signal into the generator excitation system through the automatic voltage regulator to apply an additional electric torque on the generator rotor. However, the classical design of the PSS, which relies on the linearization of a single-machine infinite-bus (SMIB) model, has two major shortcomings. First, the SMIB model is a reduced-order model by neglecting those important dynamics associated with network interconnections. It cannot adequately describe the inter-area oscillation modes due to network interconnections. Hence, the classical PSS is effective in damping local oscillation, but it may not provide enough damping to the inter-area oscillations unless carefully tuned. Furthermore, the local controller designs are independent of one another without any proper coordination among them. Second, the linearization based controller design greatly restricts the validity of the controller to the neighborhood of the operating point under consideration. When the system loading or network topology drastically changes during the normal system operation, the resulting PSS may no longer yield a satisfactory damping effect.

Another popular approach of damping inter-area oscillations is to introduce various supplementary modulation controllers to flexible AC transmission system (FACTS) devices (see, for example, (El-Moursi et al. 2010, Lerch et al. 1991, Yang et al. 1998, Zarghami et al. 2010). Although FACTS controllers can achieve a satisfactory damping effect for inter-area oscillations (Mithulananthan et al. 2003), they are not cost-effective when used only for damping control. On the other hand, FACTS controllers share the same shortcoming with the classical PSS due to the linearization-based controller design. Furthermore, the interactions between FACTS controllers and the PSSs could even potentially degrade the damping without proper coordination (Gibbard et al. 2000).

The use of high-voltage DC (HVDC) lines for damping inter-area oscillations is attracting consistent attention from both academia and industry. This is achieved by modulating the active power transfer over the HVDC line. Several modulation control strategies for HVDC lines were proposed in (Harnefors et al. 2014) and (Pipelzadeh et al. 2010). Although good performance was demonstrated on a particular oscillation mode, the proposed modulation methods usually ignored the fact that modulation control for one mode may adversely impact the other inter-area oscillation modes.

To overcome the above-mentioned issues for active damping of inter-area oscillations, there have been persistent efforts to determine appropriate global signals as the control input of proposed damping controllers as in (Aboul-Ela et al. 1996) and (Farsangi et al. 2004). Because the feedback of global signals actually establishes the correlation among independent local controllers, it is more effective than the feedback of local signals only. These efforts have been particularly facilitated by the technology of wide area measurement system (WAMS) enabled by the development of phasor measurement units (PMUs). Many WAMS-based damping controllers have been developed (see, for example, (Kamwa et al. 2001, Li et al. 2012, Trudnowski et al. 2013, Zhang and Bose 2008). In this project, we develop a universal wide-area damping control as conceptually shown in Figure 2, where the power system (i.e., the "plant") is denoted by $G_p(s)$, the damping controller (i.e., the "control") by $G_c(s)$ and the WAMS (i.e., the "feedback") by $H(s)$. The proposed universal damping control can use a mix of various fast-acting resources existing in both transmission and distribution systems such as PSS, FACTS devices, HVDC lines, and even end-use loads to effectively mitigate the inter-area oscillations. In this project, the HVDC lines and end-use loads are investigated for the implementation of proposed universal damping control in particular. Furthermore, to avoid undesirable adverse damping interactions among different modes, a rigorous method for real-time modal decomposition based on PMU measurements is proposed to facilitate the development of decoupled damping control.

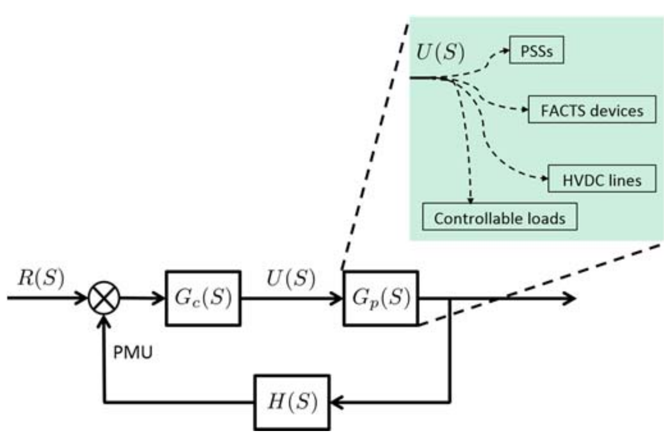

Figure 2. Conceptual Illustration of Proposed Universal Wide-area Damping Control

2.0 Universal Damping Control

In most cases, inter-area oscillations are usually caused by transferring large amounts of real power between two interconnected areas. Thus, it is a straightforward way to control the real power in the system for the oscillation mitigation. However, most existing damping controllers introduce additional damping to the inter-area oscillation modes through either a generation excitation system (e.g., PSS) or transmission line (e.g., FACTS), which actually affects the real power indirectly. Some of the work that directly affects the real power to damp the inter-area oscillations has been reported in (Huang et al. 2010, Neely et al. 2013, Pal et al. 2000); and (Pierre et al. 2016).

In (Huang et al. 2010), a Modal Analysis for Grid Operations (MANGO) procedure was established to enable grid operators to immediately mitigate inter-area oscillations by adjusting system operating conditions, where the detection of low damping is achieved by the modal analysis with real-time phasor measurements. However, the MANGO procedure can enact as part of a remedial action scheme rather than as an active damping control. In (Pal et al. 2000), robust damping controllers were designed for superconducting magnetic energy storages to enhance the damping of multiple inter-area modes by injecting real power into the system. In (Neely et al. 2013) and (Pierre et al. 2016), two damping control systems using ultracapacitor-based energy storage and HVDC lines for real power injection were designed for areas expected to oscillate against one another. Although the idea of directly modulating the real power has been shown to be effective in damping inter-area oscillations, the practical applicability of proposed damping controllers could be limited due to the availability of energy storages (Neely et al. 2013, Pal et al. 2000) and HVDC lines (Pierre et al. 2016). Therefore, it is necessary to develop a universal damping control that can be easily implemented by different fast-acting resources that are geographically dispersed within both the transmission and distribution systems for the damping of inter-area oscillations.

Inter-area oscillations are usually observed in the power system with geographical areas connected by relatively weak tie-lines. When there is large amount of power transfer between weakly-coupled areas, power oscillations of 0.1 Hz to 1.0 Hz can be initiated even by a small disturbance anywhere in the power system. It involves a group of generators on one side of the tie-line oscillating against another group of generators on the other side. When remote measurements become available through the WAMS, a simple but effective wide-area damping control can be designed to mitigate inter-area oscillations between two areas as illustrated in Figure 3, where the power transfer is flowing from Area One to Area Two.

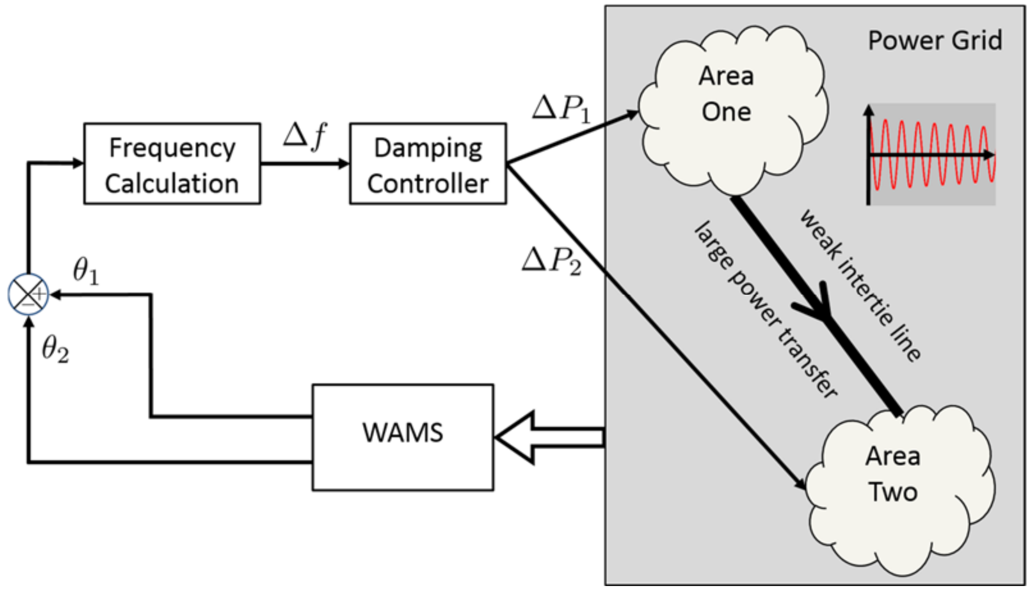

Figure 3. Schematics of the Universal Damping Control Strategy

Let θ_1 and θ_2 denote the voltage phase angles of any two buses in Areas One and Two, respectively. For convenience, these two buses can be selected as those connected by the tie-line between two areas. With the measurements of phase angles, the corresponding bus frequencies, f_1 and f_2, can be calculated. When there are inter-area oscillations, the frequency difference between f_1 and f_2 will be nonzero. When f_1 is greater than f_2 at any time instance, it implies that Area One is sending excessive power to Area Two. In order to reduce the difference between f_1 and f_2, the following actions can be taken either individually or in combination:

1. Reduce power supply or increase power demand in Area One.

2. Increase power supply or reduce power demand in Area Two.

3. Inject reverse power flow to the tie-line directly without changing power supply and demand.

Hence, the frequency difference serves as an excellent indicating signal and can be used as the negative feedback in the following damping controllers for real power supply modulation in individual areas,

$$\Delta P_1 = -K_1(f_1 - f_2) \tag{1}$$

and

$$\Delta P_2 = -K_2(f_2 - f_1) \tag{2}$$

where $K_1, K_2 > 0$ are the controller gains.

The wide-area damping control as defined by (1) and (2) is actually universal because it can be implemented in practice by various fast-acting resources existing in either area as long as there are appropriate resource-level control strategies to deliver the desired ΔP_1 and ΔP_2. In other words, different types of resources can be deployed in different areas to effectively damp the inter-area oscillations. This greatly resolves the availability issue of applying the damping control that is specific to a particular type of resources. This universal damping control has been implemented by energy storage in (Neely et al. 2013) and a single HVDC line in (Pierre et al. 2016). The implementation by multiple HVDC lines and end-use loads are presented in Sections 3.0 and 4.0, respectively.

Since the proposed universal damping control relies on real-time feedback of directly measured signals, it may not be effective in damping all of the oscillation modes in the system. In the worst case, the damping of two modes could be affected in the opposite directions, which is very undesirable. Hence, a rigorous method for real-time modal decomposition based on PMU measurements is presented in Section 5.0. With the proposed modal decomposition, the damping control for different oscillation modes can be decoupled without adverse interactions. This will significantly increase the applicability of the proposed universal wide-area damping control.

3.0 HVDC Line Modulation

HVDC power transmission systems have become increasingly popular in modern power grids. Because of their high voltage and non-skin effects, HVDC systems are economically feasible and electrical losses are lower than those of conventional AC systems for bulk power transmission over long distances. The HVDC line can deliver electricity generated by renewable resources to the main grid more efficiently, and transfer bulk power between unsynchronized AC transmission systems. As a promising transmission technology, HVDC systems are the key to the future power grid.

The power flow over the HVDC lines can be controlled independently of the phase angle between the source and load. Therefore, HVDC lines have been studied to solve the issue of inter-area oscillations in the power grid, and many studies have shown that the oscillation of low frequencies can be damped by adding a controlled HVDC line in parallel with the existing resonating AC line (Dougherty and Hillesland 1970, Harley and Balda 1985, Piwko and Larsen 1982). In the 1970s, researchers noticed that properly controlling the current regulator at the sending terminal of the Pacific DC Intertie (PDCI) can increase the damping of the small-signal swing mode of AC interties (Cresap and Mittelstadt 1976). The control algorithm is very simple and only based on the rate of change of AC intertie power, and the installation of a telecommunication link if preferred (Cresap et al. 1978). Currently, wide-area damping control as defined by (1) and (2) is being experimentally investigated (a prototype controller has recently been put in operation) using the PDCI (Pierre et al. 2016, Schoenwald et al. 2017, Trudnowski et al. 2013). It is concluded that modulation of ±100 MW to ±200 MW is enough to provide significant damping.

The growing use of and increased interest in HVDC lines around the world opens the possibility to not only consider control on a line-by-line basis, but also to study the coordinated control of several HVDC lines at the same time. In addition to the PDCI, there are still other HVDC lines in the Western Electricity Coordination Council (WECC) system including the existing Intermountain Power Project (IPP), and the proposed TransWest Express transmission project (TWE). In this project, we investigate the simultaneous use of these HVDC lines for inter-area oscillation damping. The simulation results show that different oscillation modes across several areas in the WECC system can be damped simultaneously by designing appropriate coordinated control strategies.

3.1 HVDC System Modeling

The proposed universal damping controller described in Section 2.0 is independent of the type of HVDC line. In other words, this controller can be implemented on an HVDC power transmission system using either a line commutated converter (LCC) or a voltage source converter. In the following, the most common LCC-HVDC line is considered as an example.

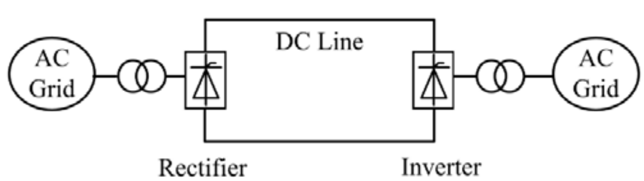

Figure 4. Illustration of a Two-terminal LCC-HVDC System

A diagram of a two-terminal LCC-HVDC system is shown in Figure 4. It consists of a controlled rectifier and inverter at the respective terminals, both of which are fed from tap-changing transformers. The rectifier converts the AC to DC and the inverter converts the DC to AC. The terminal voltages of the HVDC line are obtained from (Ni and Fouad 1987) and (Zhou et al. 2011) as follows:

$$V_{\mathrm{dc,rec}} = \frac{3\sqrt{2}}{\pi} N_B V_{B,\mathrm{rec}} \cos\alpha - R_c I_{\mathrm{dc,rec}} \tag{3}$$

and

$$V_{\mathrm{dc,inv}} = \frac{3\sqrt{2}}{\pi} N_B V_{B,\mathrm{inv}} \cos\beta - R_c I_{\mathrm{dc,inv}}, \tag{4}$$

where N_B is the number of converter bridges, $V_{B,\mathrm{rec}}$ and $V_{B,\mathrm{inv}}$ are the base voltages of the transformer secondary side, α and β are the firing angles of the converters, $I_{\mathrm{dc,rec}}$ and $I_{\mathrm{dc,inv}}$ are the DC currents, and R_c is the equivalent commutation resistance, which is

$$R_c = \frac{3}{\pi} N_B X_c, \tag{5}$$

where X_c is the equivalent commutation reactance. The magnitude of the AC current is related to the DC current as specified by the following,

$$|I_{\mathrm{ac}}| = I_{\mathrm{dc}} N_B \frac{\sqrt{6}}{\pi}. \tag{6}$$

In normal operation, the voltage of a two-terminal HVDC line is set by the inverter controller, and the current (or active power) is set by the rectifier controller. To avoid commutation failures, the extinction angle of the inverter is determined as follows,

$$\gamma = 180^{\mathrm{o}} - \alpha - \mu, \tag{7}$$

where γ is the overlap angle. The DC line models are represented by a T-equivalent as:

$$L_{\mathrm{dc}} \frac{\mathrm{d}}{\mathrm{d}t} I_{\mathrm{dc,rec}} = V_{\mathrm{dc,rec}} - R_{\mathrm{dc}} I_{\mathrm{dc,rec}} - V_c \tag{8}$$

$$L_{\mathrm{dc}} \frac{\mathrm{d}}{\mathrm{d}t} I_{\mathrm{dc,inv}} = -\left(V_{\mathrm{dc,inv}} - R_{\mathrm{dc}} I_{\mathrm{dc,inv}} - V_c\right) \tag{9}$$

$$C_{\mathrm{dc}} \frac{\mathrm{d}}{\mathrm{d}t} V_c = I_{\mathrm{dc,rec}} - I_{\mathrm{dc,inv}}, \tag{10}$$

where R_{dc}, C_{dc}, L_{dc}, and V_c are the equivalent DC line resistance, capacitance, inductance, and DC voltage. The power factor pf at the equivalent source bus is

$$pf = \cos\alpha - \frac{R_c I_{\mathrm{dc}}}{|V_{\mathrm{ac}}|}. \tag{11}$$

Consequently, the active and reactive power of the HVDC converter can be obtained as shown in (Borovikov et al. 2016),

$$P = V_{\mathrm{dc}} I_{\mathrm{dc}} \tag{12}$$

$$Q = P \times \tan\left(\cos^{-1}\left(\frac{\cos\alpha + \cos(\pi - \gamma)}{2}\right)\right) \tag{13}$$

3.2 Controllability Exploration

For the LCC-HVDC line, the real power flows from the rectifier to the inverter, where the rectifier controls the DC line current and the inverter controls the DC voltage. When it is used to implement the proposed universal damping control, the modulation of real power over the HVDC line is achieved by controlling the line current through the rectifier. Therefore, the power modulation signal for the power sending area as defined by (1) has to be converted into a current signal. Furthermore, the frequency measurements of both areas can be simply taken from both ends of the HVDC line. Hence, the current modulation signal for a single HVDC line to damp inter-area oscillations can be defined as

$$I_{\mathrm{rec}} = -K(f_{\mathrm{rec}} - f_{\mathrm{inv}}), \tag{14}$$

where $K > 0$ is the controller gain.

Note that the damping control defined by (14) can be implemented by any single HVDC line for individual power modulation. However, when there are multiple HVDC lines with more than two areas involved, coordinated modulation of HVDC lines could be more effective for inter-area oscillation damping than individual modulation. The frequency difference between two terminals of one HVDC line as in (14) may not be the only choice of the feedback signal for current control. There are actually many different ways of constructing the feedback signal based on the geographical locations of these HVDC lines. In this following, the coordinated modulation of multiple HVDC lines is investigated by exploring different choices of feedback signals.

We consider a modified version of the minniWECC system given in (Trudnowski 2008) as our test system. The minniWECC system is a reduced-order dynamic model of the WECC system in North America. It retains the overall inter-area modal properties of the WECC system and thus is suitable for testing inter-area oscillation mitigation strategies. This test system contains 34 generators, 120 buses, 115 lines and high voltage transformers, 54 generator and load transformers, 19 load buses, and 2 HVDC transmission lines. There are several inter-area oscillation modes in the minniWECC system, whose frequencies and damping ratios actually depend on the operating condition of the system. This modified minniWECC system has three HVDC lines as shown in Figure 5. This first HVDC line is the PDCI (red), which transmits 2850 MW at ±500 kV DC from northwest to the southwest. The second one is the IPP (blue), which transmits 1900 MW at ±500 kV DC from mid-east to the southwest. The PDCI and IPP were modeled in the original minniWECC system as simple positive and negative loads. Their models are replaced with more detailed dynamic models in this work. It is also noted that the location of the inverters of the PDCI and IPP are very close to each other. The third one is the TWE (green), which transmits 2500 MW at ±600 kV DC from east to the mid-southwest. It is added to the system location as specified by the real transmission plan. Because there are three HVDC lines in the system, we have three current modulation signals and six frequency measurements with two terminal measurements from each line. Then, the coordinated modulation of three HVDC lines can be described by the following current control,

$$\begin{bmatrix} I_{\mathrm{rec},1} \\ I_{\mathrm{rec},2} \\ I_{\mathrm{rec},3} \end{bmatrix} = \boldsymbol{K} \begin{bmatrix} f_{\mathrm{rec},1} \\ f_{\mathrm{inv},1} \\ f_{\mathrm{rec},2} \\ f_{\mathrm{inv},2} \\ f_{\mathrm{rec},3} \\ f_{\mathrm{inv},3} \end{bmatrix}, \tag{15}$$

where $I_{\mathrm{rec},i}$, $f_{\mathrm{rec},i}$, and $f_{\mathrm{inv},i}$ are the current modulation signal, and terminal frequency measurements of the i-th HVDC line, respectively, and the matrix $\boldsymbol{K} \in \mathbb{R}^{6\times 6}$ describes the specific way of combining frequency measurements as the feedback signal. In the following, three different coordinated control designs are introduced, which lead to three different choices of $\boldsymbol{K}$.

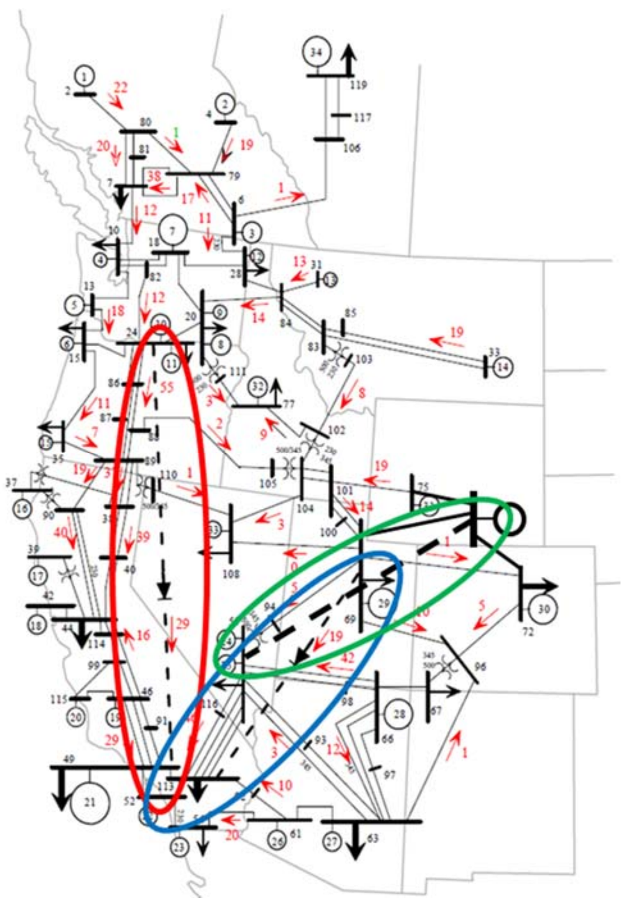

Figure 5. Modified minniWECC System with Three HVDC Lines

A. Design One (D1)

In this design, three HVDC lines are individually controlled. That is, their line currents are modulated independently by applying the current control defined in (14). In this case, the matrix $\boldsymbol{K}$ becomes block diagonal, and the coordinated control (15) takes the following form,

$$\begin{bmatrix} I_{\text{rec},1} \\ I_{\text{rec},2} \\ I_{\text{rec},3} \end{bmatrix} = \begin{bmatrix} -K_1 & K_1 & 0 & 0 & 0 & 0 \\ 0 & 0 & -K_2 & K_2 & 0 & 0 \\ 0 & 0 & 0 & 0 & -K_3 & K_3 \end{bmatrix} \begin{bmatrix} f_{\text{rec},1} \\ f_{\text{inv},1} \\ f_{\text{rec},2} \\ f_{\text{inv},2} \\ f_{\text{rec},3} \\ f_{\text{inv},3} \end{bmatrix}, \tag{16}$$

where $K_1, K_2, K_3 > 0$ are the controller gains. This control design ignores the possible interactions among different HVDC lines. If the connected areas by one HVDC line do not overlap with those by the other line, the control defined by (16) is the only choice. Otherwise, there could be more choices of $\boldsymbol{K}$ by taking into account how the connected areas are overlapped with each other.

B. Design Two (D2)

Because the physical location of the inverters of the PDCI and IPP are very close to each other, it can be well imagined that there exists a virtual HVDC line between the rectifiers of both PDCI and IPP. If this virtual HVDC line is used for inter-area oscillation damping by itself, the coordinated control (15) takes the following form, assuming the power transfer over the PDCI is larger than that over the IPP,

$$\begin{bmatrix} I_{\text{rec},1} \\ I_{\text{rec},2} \\ I_{\text{rec},3} \end{bmatrix} = \begin{bmatrix} -K_4 & 0 & K_4 & 0 & 0 & 0 \\ K_4 & 0 & -K_4 & 0 & 0 & 0 \\ 0 & 0 & 0 & 0 & 0 & 0 \end{bmatrix} \begin{bmatrix} f_{\text{rec},1} \\ f_{\text{inv},1} \\ f_{\text{rec},2} \\ f_{\text{inv},2} \\ f_{\text{rec},3} \\ f_{\text{inv},3} \end{bmatrix} \tag{17}$$

where $K_4 > 0$ is the controller gain. It follows from (17) that the sum of modulated DC currents flowing into southwest through the PDCI and IPP, respectively, will be zero. Because the inverters control the DC voltages to be constants, the southwest should not see any power modulation. Instead, power modulation will be mostly observed between the northwest and the mid-east.

C. Design Three (D3)

If the virtual HVDC line between the rectifiers of both PDCI and IPP is considered along with their HVDC lines, there are a total of four lines to be coordinated for inter-area oscillation damping. Hence, the first and second designs can be combined, leading to the following coordinated control,

$$\begin{bmatrix} I_{\mathrm{rec},1} \\ I_{\mathrm{rec},2} \\ I_{\mathrm{rec},3} \end{bmatrix} = \begin{bmatrix} -K_1 - K_4 & K_1 & K_4 & 0 & 0 & 0 \\ K_4 & 0 & -K_2 - K_4 & K_2 & 0 & 0 \\ 0 & 0 & 0 & 0 & -K_3 & K_3 \end{bmatrix} \begin{bmatrix} f_{\mathrm{rec},1} \\ f_{\mathrm{inv},1} \\ f_{\mathrm{rec},2} \\ f_{\mathrm{inv},2} \\ f_{\mathrm{rec},3} \\ f_{\mathrm{inv},3} \end{bmatrix} \tag{18}$$

where $K_1, K_2, K_3, K_4 > 0$ are controller gains. In this way, the first and second designs can complement each other for better damping of inter-area oscillations.

3.3 Simulation Results

In the following, simulation studies are performed to evaluate the effectiveness of the above three coordinated control designs. The modified minniWECC system shown in Figure 5 is used as the test system, which includes 35 generators, 122 buses, and more than 6 inter-area oscillation modes. At time t = 2.0 seconds, Generator 33 is suddenly tripped to create a large disturbance and trigger inter-area oscillations in the system with many modes. The controller gains K_1, K_2, K_3 and K_4 in (16)–(18) are selected to be 3000, 1500, 1500, and 3000 kA/Hz, respectively.

Figure 6 shows the inter-area oscillations observed from the power flow over line 89-38, which is an AC tie-line in parallel with the PDCI. It can be seen that all three control designs enhance the damping of the inter-area oscillations observed over this line. In particular, the effectiveness of the second and third designs is better than that of the first design.

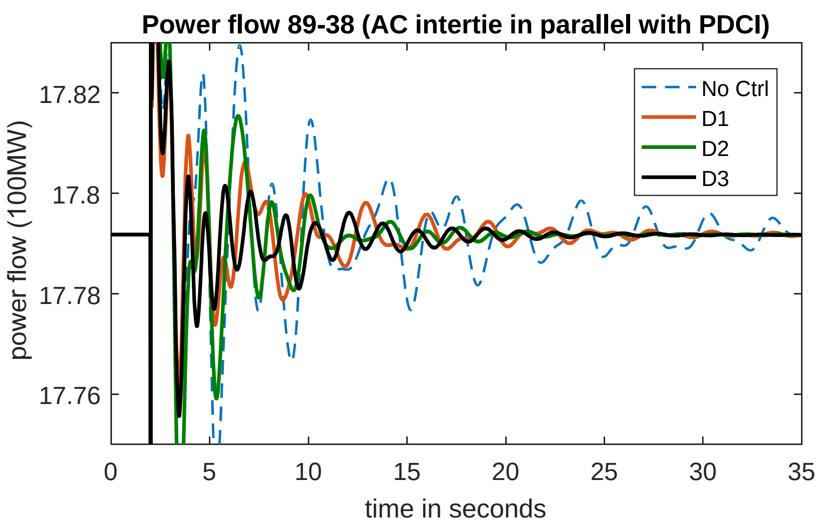

Figure 6. Power Flow over AC Tie-line 89-38

Figure 7 shows the inter-area oscillations observed from the power flow over line 57-113, which is an AC tie-line in parallel with the IPP. It can be seen that all three control designs enhance the damping of the inter-area oscillations observed over this line. In particular, the effectiveness of the first and second designs is similar, while the third design appears to be better than the other two.

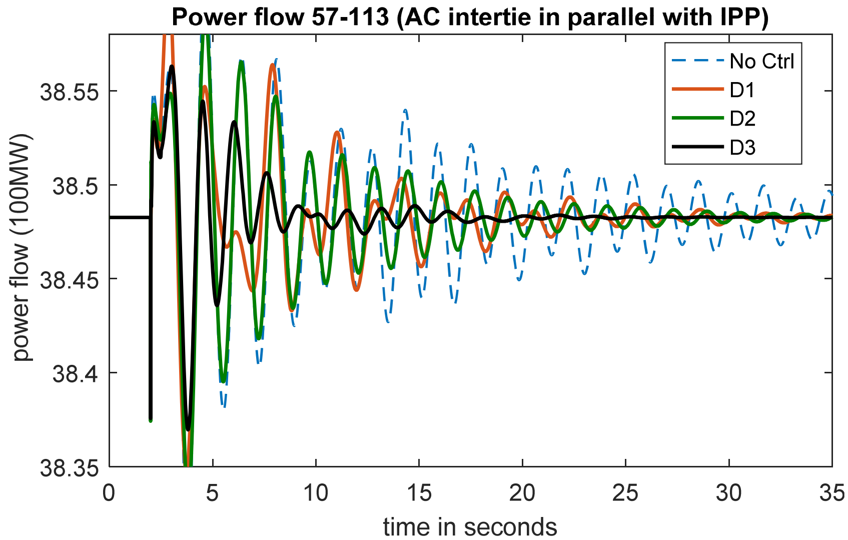

Figure 7. Power Flow over AC Tie-line 57-113

Figure 8 shows the inter-area oscillations observed from the power flow over line 94-69, which is an AC tie-line in parallel with the TWE. It can be seen that all three control designs enhance the damping of the inter-area oscillations observed over this line. In particular, the effectiveness of the first and third designs is better than that of the second design.

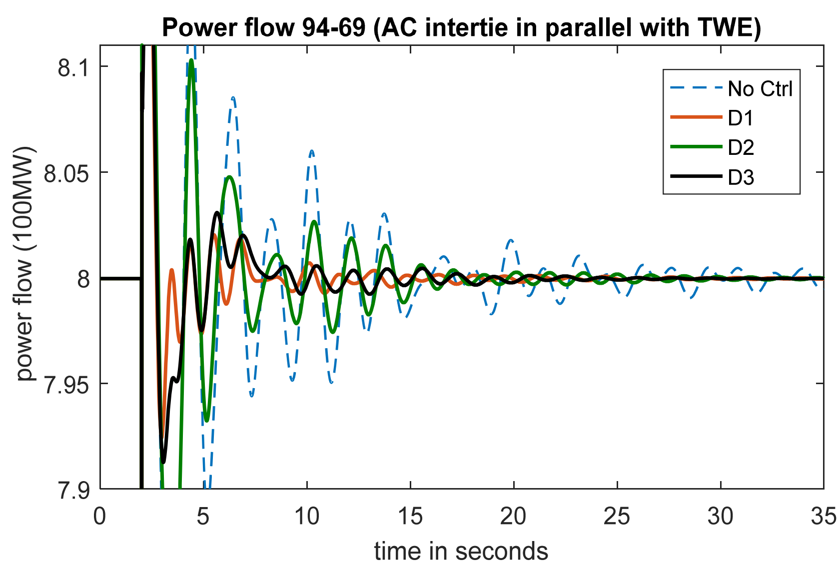

Figure 8. Power Flow over AC Tie-line 94-69

Figure 9 shows the inter-area oscillations observed from the power flow over line 102-77, which is an AC tie-line in parallel between the rectifiers of the PDCI and IPP. It can be seen that all three control designs enhance the damping of the inter-area oscillations observed over this line. In particular, the effectiveness of the third design is better than that of the first and second designs.

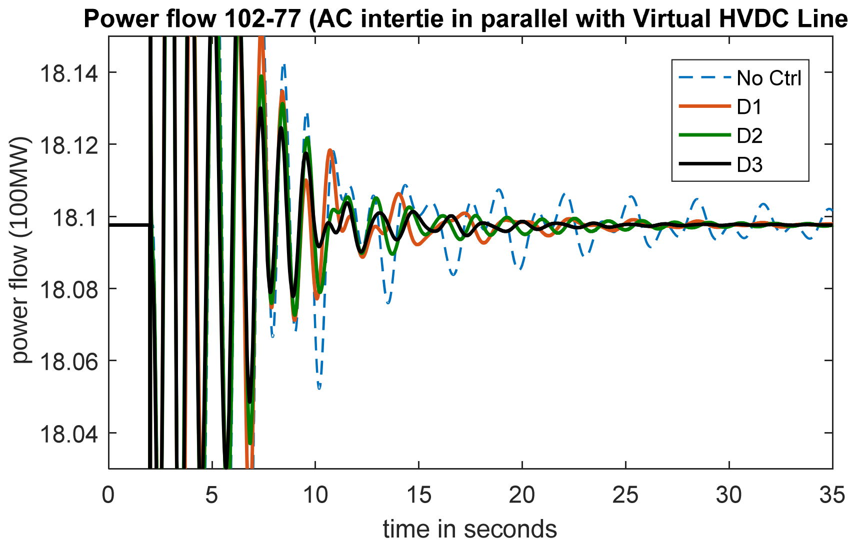

Figure 9. Power Flow over AC Tie-line 102-77

Table 1 summarizes the damping ratios of dominant inter-area oscillation modes, which are obtained by applying a Prony's algorithm based analysis tool (Etingov et al. 2017) on the above power flows over four AC tie-lines. Note that the calculated damping ratios for the same mode may differ (in a small range) due to the different locations of power flow measurements.

In Observation 1 of Table 1, corresponding to oscillations observed from power flow of line 89-38 in Figure 5, the BC mode and NSB mode are detected, while the East-West South mode is not observed due to the location and power flow direction of line 89-38 (it is not in the East-West South oscillation group). All three designs are able to increase the damping ratios of the oscillation modes, and the second and third designs provide a higher increase, which is consistent with visual inspection of Figure 6.

In Observation 2 of Table 1, corresponding to oscillations observed from power flow of line 57-113 in Figure 5, the BC mode, NSB mode, and East-West South mode are detected. All three designs are able to increase the damping ratio of the oscillation modes, except for the second design, which cannot increase the damping ratio of East-West South mode. The third design provides a higher increase in the damping ratios, as is visually observed in Figure 7.

In Observation 3 of Table 1, corresponding to oscillations observed from power flow of line 94-69 in Figure 5, BC mode, NSB mode, and East-West South mode are detected. All three designs are able to increase the damping ratio of the oscillation modes. The first and third designs provide a higher increase of the damping ratios, as is visually verified in Figure 8.

In Observation 4 of Table 1, corresponding to oscillations observed from power flow of line 102-77 in Figure 5, the BC mode, NSB mode, and East-West South mode are detected. All three designs are able to increase the damping. The third design provides a higher increase of the damping ratios, as verified by visual inspection of Figure 9.

Table 1. Damping Ratios of Dominant Inter-area Oscillation Modes under HVDC Line Modulation

Observation 1		Damping Ratio (%)			
Mode	F (Hz)	No Ctrl	D1	D2	D3
BC	0.630	2.455	2.714	5.058	4.711
NSB	0.299	3.696	7.134	15.875	19.022
Observation 2		Damping Ratio (%)			
Mode	F (Hz)	No Ctrl	D1	D2	D3
BC	0.634	1.849	2.849	3.647	5.466
NSB	0.299	2.968	7.088	14.867	18.443
E-W S	0.851	7.738	14.002	4.876	11.313
Observation 3		Damping Ratio (%)			
Mode	F (Hz)	No Ctrl	D1	D2	D3
BC	0.635	1.593	5.868	4.376	4.870
NSB	0.300	3.432	9.019	9.554	16.730
E-W S	0.848	4.471	4.495	5.307	6.258
Observation 4		Damping Ratio (%)			
Mode	F (Hz)	No Ctrl	D1	D2	D3
BC	0.629	1.309	3.646	2.746	4.475
NSB	0.293	6.217	8.629	17.541	22.648
E-W S	0.865	5.788	6.746	8.437	8.648

4.0 Demand-side Modulation

Demand-side control has presented a novel and viable way to supplement supply-side control for the future power grid. Traditionally, the end-use loads such as air conditioners and water heaters have commonly been treated as passive and non-dispatchable. However, as pointed out in (Callaway and Hiskens 2011), end-use loads can now be actively controlled to provide various grid services such as primary frequency response (Lian et al. 2016) and secondary frequency regulation (Motalleb et al. 2016). The end-use loads usually have a large population size and fast aggregated ramping rate. When properly coordinated, the collection of end-use loads can realize the real power modulation that satisfies the requirements of speed, accuracy, and magnitude.

In this project, wide-area demand-side control is proposed to modulate the real power of end-use loads for inter-area oscillation damping. It is the first time that it has been proposed that end-use loads participate in active damping for improving the small-signal stability of the power grid. The proposed load control strategy organizes the decision-making into two different layers: the device layer and the supervisory layer. At the device layer, individual loads can turn themselves on or off independently whenever the broadcasted signals from the coordinator exceed predetermined local thresholds. At the supervisory layer, the coordinator oversees the selection of local thresholds to ensure that the aggregated load response can follow the desired real power modulation. Detailed simulation studies are performed on a reduced-order dynamic model of the WECC system to illustrate the effectiveness of the proposed wide-area demand-side control.

4.1 Control Strategy

In order to design the load control strategy for inter-area oscillation damping, we examine first the power modulation signal ΔP (ΔP_1 or ΔP_2) of the universal damping control as defined by (1) and (2). When the inter-area oscillations are effectively damped, ΔP typically exhibits a well-damped oscillation and decays to zero eventually as in Figure 10. For each red solid segment in Figure 10, where ΔP is rising, it implies that the total power supply from Area One should increase during this period. For each blue dotted segment in Figure 10, where ΔP is falling, it implies the opposite.

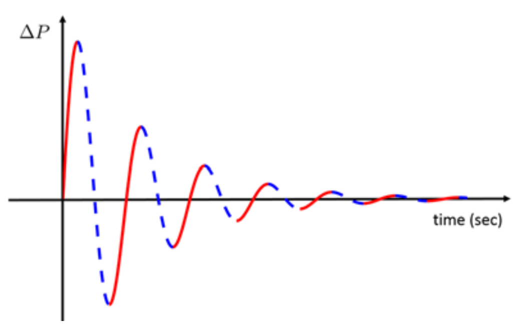

Figure 10. Illustration of a Typical Power Modulation Signal

If the increase and decrease of power supply from Area One are considered separately, ΔP can be expressed as the sum of two independent signals as shown in Figure 11. One is referred to as the rising signal ΔP^+, which dictates how the power supply should increase over time, and the other one is referred to as the falling signal ΔP^-, which dictates the opposite. If end-use loads in Area One are used to deliver the power modulation ΔP, those that are currently ON can be used to deliver ΔP^+ by turning OFF, and those that are currently OFF can be used to deliver ΔP^- by turning ON. In the following, a demand-side control with hierarchical decision-making as illustrated in Figure 12 is proposed for end-use loads to realize the real power modulation through both slow time-scale coordination and fast time-scale control.

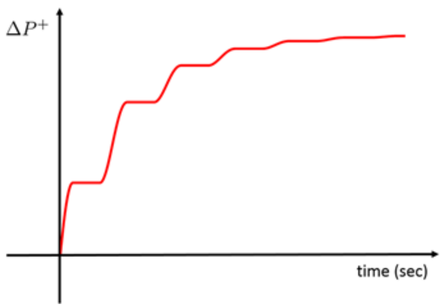

(a) Rising Signal ΔP^+

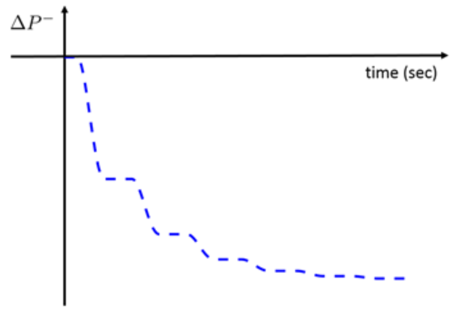

(b) Falling Signal ΔP^-

Figure 11. Decomposition of the Typical Power Modulation Signal

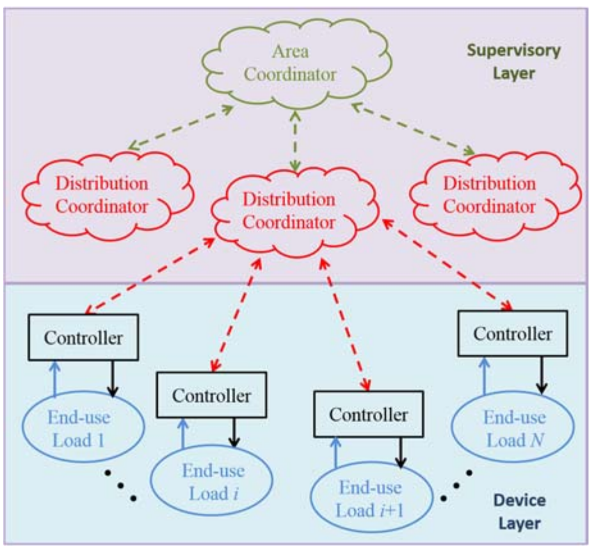

Figure 12. Diagram of Proposed Demand-side Control Strategy

4.1.1 Device-layer Control

At the device layer, individual end-use loads are equipped with a threshold-based controller as shown in Figure 13, which operates on top of the original local controllers. This threshold-based controller remains inactive until individual end-use loads participate in the service of providing active damping. When it becomes active, the threshold-based controller overrides local control logic and forces individual end-use loads to stay with their committed operating states (*ON* or *OFF*) until forced switching. In real time, it monitors the rising signal $\Delta P^+(t)$ and the falling signal $\Delta P^-(t)$ broadcasted from the supervisory layer. Whenever the broadcasted signals exceed the preset thresholds specified by p_{th}^+ and p_{th}^-, the threshold-based controller turns individual end-use loads ON ($\Delta P^- \geq p_{\mathrm{th}}^-$) or OFF ($\Delta P^+ \geq p_{\mathrm{th}}^+$) immediately, and forces them to stay with the new operating states (*OFF-LCK* or *ON-LCK*) until the end of the current engagement.

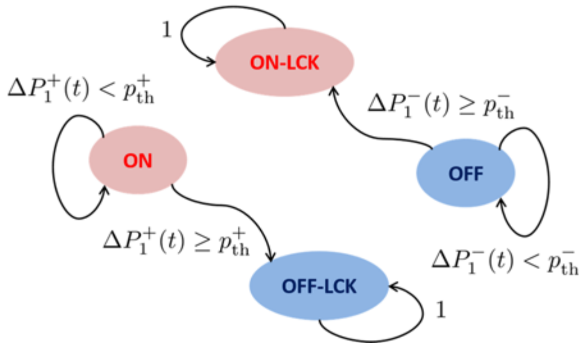

Figure 13. Schematics of the Threshold-based Control Logic

4.1.2 Supervisory-layer Coordination

At the supervisory-layer, individual end-use loads within the same distribution system are managed by the same distribution coordinator. In real time, the distribution coordinator needs to calculate the power modulation signal $\Delta P(t)$ based on the measurements provided by the WAMS, determine the rising signal $\Delta P^+(t)$ and the falling signal $\Delta P^-(t)$ by decomposing $\Delta P(t)$, and broadcast them to individual end-use loads under its authority. On the other hand, the distribution coordinator has to ensure that the aggregated load response under autonomous threshold-based control can follow the desired power modulation signal $\Delta P(t)$. This is achieved by coordinating the selection of local thresholds in different areas once every coordination period. The length of each coordination period should be a design parameter depending on the characteristics of end-use loads under consideration. Further research is necessary to determine the appropriate length of the coordination period.

At the beginning of every coordination period, individual end-use loads that are willing to provide the service of active damping for the coming period in both areas have to submit their operating states (ON or OFF) and power levels (kW) to their corresponding distribution coordinators. The distribution coordinators count the total ON power $\Delta P_{\text{max},i}^+$ and OFF power $\Delta P_{\text{max},i}^-$ in their distribution systems, and send them to the area coordinator. Then, the area coordinator determines the total ON power, $\Delta P_{1,\text{max}}^+$ and $\Delta P_{2,\text{max}}^+$, and OFF power, $\Delta P_{1,\text{max}}^-$ and $\Delta P_{2,\text{max}}^-$, for each area and send them back to the corresponding distribution coordinators. Now assume that the *i*-th distribution system belongs to Area One. Then the *i*-th distribution coordinator determines the thresholds for engaged end-use loads in the *i*-th distribution system that will be ON for the coming period as shown in Figure 14. The thresholds for engaged end-use loads that will be OFF for the coming period are determined in a similar way.

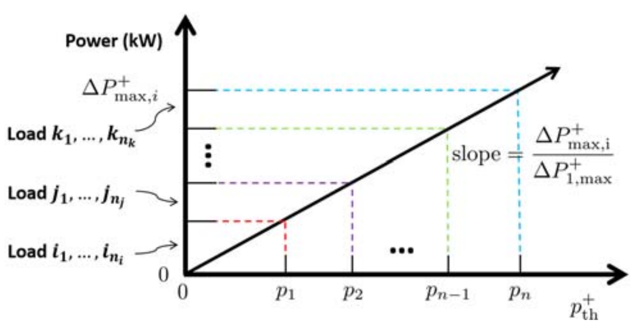

Figure 14. Schematics of Supervised Threshold Determination

4.2 Simulation Results

In the following, the effectiveness of the proposed demand-side control is illustrated by simulations on the minniWECC system (Trudnowski 2008) as shown in Figure 15. Various case studies are performed by considering different contingency events and penetration levels of controllable end-use loads. In the following simulation studies, the operating condition is selected such that the Alberta mode of 0.324 Hz is lightly damped with 0.5% damping and all the other modes are well damped as shown in Table 2. Due to the existence of the lightly damped Alberta mode, the power transfer from the north to the south exhibits underdamped oscillation upon system disturbances. Hence, it requires additional active damping in order to mitigate the inter-area oscillation between the north and the south.

Table 2. Inter-area Oscillation Modes under Consideration for Demand-side Control

Mode	Frequency (Hz)	Damping (%)
N-S	0.170	24.0
Alberta	0.324	0.5
E-W south 1	0.501	7.5
Montana	0.549	7.0
BC	0.626	2.0
E-W South 2	0.683	5.0
Middle	0.709	4.0

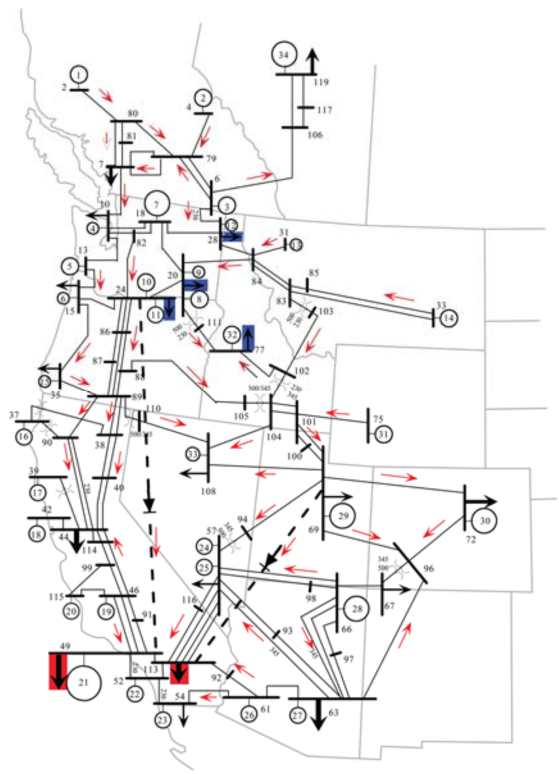

Figure 15. Schematics of minniWECC Test System

To proceed, two different contingency events are considered to initiate the underdamped power oscillation associated with the Alberta mode. The first contingency (C1) is chosen to be a sudden loss of generator 4 (1275 MW) on bus 9. The second contingency (C2) is chosen to be a three-phase fault on the 500 kV line connecting bus 89 and bus 90 followed by line tripping after three cycles. In order to mitigate the underdamped power oscillation between the north and south areas, water heaters are considered as the controllable end-user loads to realize the universal damping control. They are located in the distribution systems represented by six load buses in Figure 15. These load buses are highlighted in blue (buses 21, 26, 29, and 78) and red (buses 50 and 112), respectively, to indicate that they belong to different areas, where blue represents the north and red the south. Different case studies are performed to evaluate the effectiveness of the proposed wide-area demand-side control. In the first case (Case 1), demand-side control is implemented with low penetration of controllable water heaters (2 GW in each area). This case represents the scenario that there are only a limited number of controllable end-user loads for oscillation damping. Hence, the corresponding damping effectiveness is also expected to be limited. In the second case (Case 2), higher penetration of controllable water heaters (5 GW in each area) is simulated to ensure there is a sufficient amount of controllable loads for oscillation damping. Thus, the damping effectiveness in Case 2 should be better than Case 1. Both Case 1 and Case 2 are compared to the base case (Case 0) without any demand-side control. To implement the damping control, the voltage phase angles of bus 24 and bus 49 are assumed to be measured by the WAMS. Then the frequency difference between these two buses are used to calculate the desired power modulation signals as defined in (1) and (2), respectively. The controller gains K_1 and K_2 are selected to be 100 p.u./Hz, which is shown to provide satisfactory damping in a reasonable amount of time. During the simulation, the contingency events occur at 1 second and the demand-side control is enabled at 10 seconds.

For C1, the tie-line power flow from bus 89 to bus 38 for each case is plotted in Figure 16. The evolution of the percentages of engaged water heaters that become ON-LCK and OFF-LCK, respectively, are shown in Figure 17. Similar plots are obtained for C2 as in Figure 18 and Figure 19. It can be seen from Figure 16 and Figure 18 that for both contingencies, the case with sufficient end-user loads (Case 2) can damp the inter-area oscillation successfully with the demand-side control. In the case with insufficient end-user loads (Case 1), the oscillation still exists, although with smaller magnitudes, at the end of the simulation because the number of available water heaters runs out before the inter-area oscillation is fully damped.

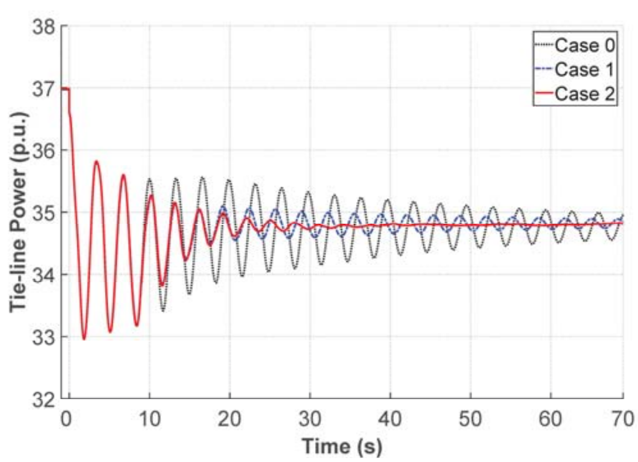

Figure 16. Comparison of Tie-line Power Flows in Different Cases under C1

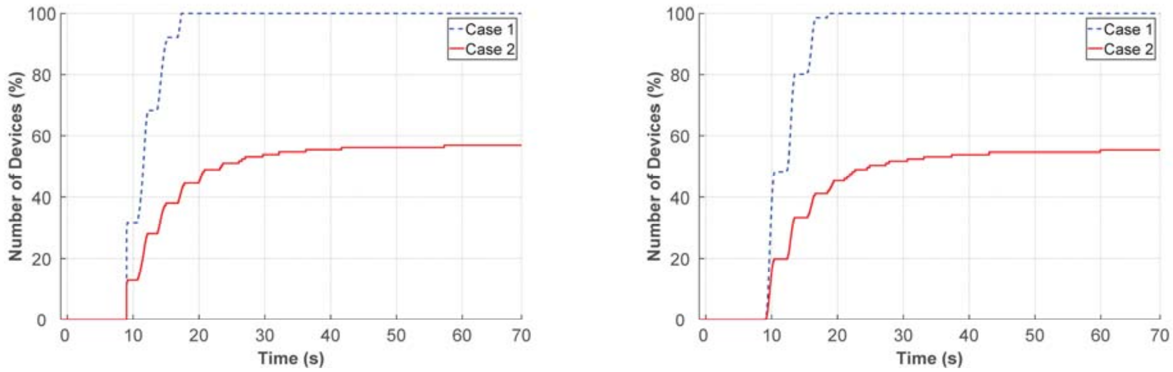

(a) ON-LCK (b) OFF-LCK

Figure 17. Evolution of the Percentage of Locked Water Heaters under C1

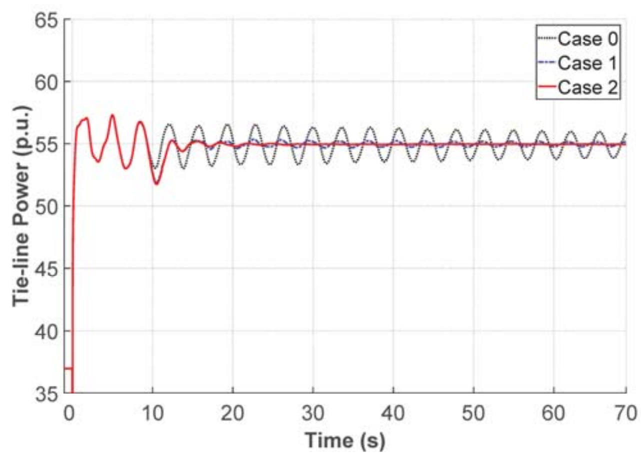

Figure 18. Comparison of Tie-line Power Flows in Different Cases under C2

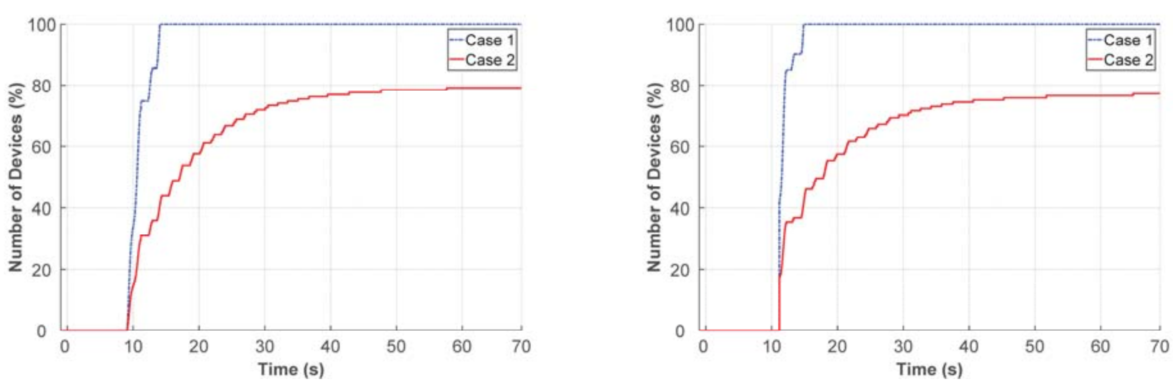

(a) ON-LCK (b) OFF-LCK

Figure 19. Evolution of the Percentage of Locked Water Heaters under C2

5.0 Modal Decomposition

For large-scale interconnected power grids, there are usually multiple inter-area oscillation modes. The universal damping control defined by (1) and (2) is designed based on the real-time feedback of directly measured frequency signals from the corresponding areas. However, not all of the modes can be observed from the measured frequency signals. The number of modes available in one frequency signal greatly depends on where the signal is measured. Therefore, the universal damping control is not guaranteed to be effective in damping all of the modes. In the worst case, the damping affects the two different modes in opposite directions. That is, when the control successfully increases the damping of one mode, it adversely decreases the damping of the other unintentionally.

To overcome this issue, the idea of modal decomposition was proposed in (Zhang et al. 2012) to damp each inter-area oscillation mode independently, that is, to realize decoupled damping control. In particular, it applied a second-band band-pass filter to extract the inter-area oscillation modal signals of concern, and used them as the feedback signals to damp the corresponding inter-area oscillation modes. It was shown in (Zhang et al. 2012) hat the proposed decoupled damping control based on modal decomposition can achieve better performance than the traditional designs based on directly measured signals. However, there are still two more issues to be further addressed. The first issue is that the signal fed to the band-pass filter is measured from only one location, and it may not represent the inter-area oscillation modes of concern very well. If the oscillation modal signal of concern has a very small magnitude in the measured signal, then it will be hard to extract by the band-pass filter due to measurement noises. The second issue is that when the frequencies of two inter-area oscillation modes are very close to each other, it is very hard to accurately separate them through the band-pass filter.

In this project, a rigorous method for real-time modal decomposition based on PMU measurements is proposed to facilitate the development of decoupled damping control. Unlike the band-pass filter used in (Zhang et al. 2012) the proposed method can extract pure oscillation modal signals more effectively. Moreover, the modal decomposition is based on the PMU measurements from different locations, which ensures the success of extracting the inter-area oscillation modes of concern. The simulation results demonstrate the effectiveness of the proposal modal decomposition by applying to the HVDC line modulation to achieve decoupled damping control of inter-area oscillation modes.

5.1 Decoupled Damping Control

The idea of decoupled damping control was first proposed in (Zhang et al. 2012). In this section, we briefly summarize the underlying principles behind this idea. To proceed, consider the following single-input single-output system for oscillation damping,

$$\begin{cases} \dot{\boldsymbol{x}}(t) = \boldsymbol{A}\boldsymbol{x}(t) + \boldsymbol{b}u(t) \\ y(t) = \boldsymbol{c}\boldsymbol{x}(t) \end{cases}, \tag{19}$$

where $\boldsymbol{x} \in \mathbb{R}^n$ is the state vector of the system, $\boldsymbol{A} \in \mathbb{R}^{n\times n}$ is the system transition matrix, $u \in \mathbb{R}$, $y \in \mathbb{R}$, $\boldsymbol{b} \in \mathbb{R}^n$ and $\boldsymbol{c} \in \mathbb{R}^{1\times n}$ are the input, output, input and output matrices, respectively. Applying the Laplace transform to (19) with zero initial conditions, i.e., $\boldsymbol{x}(0) = \boldsymbol{0}$, we have

$$\begin{cases} s\boldsymbol{X}(s) = \boldsymbol{A}\boldsymbol{X}(s) + \boldsymbol{b}U(s) \\ Y(s) = \boldsymbol{c}\boldsymbol{X}(s) \end{cases}. \tag{20}$$

For the simplicity of the following derivation, we assume that $\boldsymbol{A}$ has n distinct eigenvalues; that is, $\boldsymbol{A}$ is diagonalizable. Let $\lambda_i \in \mathbb{C}$ denote the i-th eigenvalue of $\boldsymbol{A}$, and let $\boldsymbol{v}_i \in \mathbb{C}^n$ and $\boldsymbol{w}_i \in \mathbb{C}^{1\times n}$ denote the right and left eigenvectors associated with λ_i, respectively. Define $\boldsymbol{T} = \begin{bmatrix} v_1 & \cdots & v_n \end{bmatrix}$ and $\Lambda = \mathrm{diag}\begin{bmatrix} \lambda_1 & \cdots & \lambda_n \end{bmatrix}$. Then, it follows that $\boldsymbol{T}^{-1}\boldsymbol{A}\boldsymbol{T} = \Lambda$ and $\boldsymbol{T}^{-1} = \begin{bmatrix} w_1^* & \cdots & w_n^* \end{bmatrix}^{\mathrm{T}}$, where ω_i^* denotes the complex conjugate of ω_i. To proceed, define the new state vector $\boldsymbol{Z} \in \mathbb{R}^n$ as

$$\mathbf{Z}(s) = \boldsymbol{T}^{-1}\boldsymbol{X}(s), \tag{21}$$

whose elements $Z_i(s)$, $i = 1, \ldots, n$, are the pure modal signals. Substituting (21) into (20), it follows that

$$\begin{cases} s\boldsymbol{Z}(s) = \Lambda\boldsymbol{Z}(s) + \boldsymbol{T}^{-1}\boldsymbol{b}U(s) \\ Y(s) = \boldsymbol{c}\boldsymbol{T}\boldsymbol{Z}(s) \end{cases}. \tag{22}$$

It follows from (22) that $Y(s)$ can be expressed as a combination of different modal signals,

$$Y(s) = \boldsymbol{c}\sum_{i=1}^{n} \boldsymbol{v}_i Z_i(s) = \sum_{i=1}^{n} Y_i(s)$$

where $Y_i(s) = \boldsymbol{c}\boldsymbol{v}_i Z_i(s)$. Now assume that $Y_i(s)$ $(1 \le i \le n)$ can be perfectly extracted from $Y(s)$ and is used as the feedback signal for the controller, that is,

$$U(s) = P(s)Y_i(s) = P(s)\boldsymbol{c}\boldsymbol{v}_i Z_i(s), \tag{23}$$

where $P(s)$ represents the controller transfer function. Substituting (23) into (22), it follows that

$$\begin{aligned} s\boldsymbol{Z}(s) &= \Lambda\boldsymbol{Z}(s) + \boldsymbol{T}^{-1}\boldsymbol{b}U(s) \\ &= \Lambda\boldsymbol{Z}(s) + \boldsymbol{T}^{-1}\boldsymbol{b}P(s)\boldsymbol{c}\boldsymbol{v}_i Z_i(s) \\ &= \Lambda\boldsymbol{Z}(s) + \boldsymbol{T}^{-1}\boldsymbol{b}\begin{bmatrix} 0 & \cdots & P(s)\boldsymbol{c}\boldsymbol{v}_i & \cdots & 0 \end{bmatrix}\boldsymbol{Z}(s) \\ &= \boldsymbol{A}_c\boldsymbol{Z}(s) \end{aligned},$$

where

$$
\boldsymbol{A}_c = \begin{bmatrix} \lambda_1 & 0 & \cdots & \boldsymbol{w}_1^* \boldsymbol{b} P(s) \boldsymbol{c} \boldsymbol{v}_i & \cdots & 0 \\ 0 & \lambda_2 & \cdots & \boldsymbol{w}_2^* \boldsymbol{b} P(s) \boldsymbol{c} \boldsymbol{v}_i & \cdots & 0 \\ \vdots & \vdots & \ddots & \vdots & \ddots & \vdots \\ 0 & 0 & \cdots & \lambda_i + \boldsymbol{w}_i^* \boldsymbol{b} P(s) \boldsymbol{c} \boldsymbol{v}_i & \cdots & 0 \\ \vdots & \vdots & \ddots & \vdots & \ddots & \vdots \\ 0 & 0 & \cdots & \boldsymbol{w}_n^* \boldsymbol{b} P(s) \boldsymbol{c} \boldsymbol{v}_i & \cdots & \lambda_n \end{bmatrix}. \tag{24}
$$

It can be seen from (24) that the feedback control (23) based on the pure modal signal $Y_i(s)$ affects the i-th mode λ_i only. Therefore, if we would like to improve the damping of a specific oscillation mode, it is necessary to extract the corresponding pure oscillation modal signal as the feedback signal for the implementation of decoupled damping control.

5.2 Wide-area Modal Decomposition

In order to design decoupled damping control, we propose a novel approach to extract the oscillation modal signals from real-time PMU measurements from different locations. Compared to the approach of using the band-pass filter, the proposed approach is capable of extracting pure oscillation modal signals in a rigorous manner. This is achieved in two steps: (1) establish the mapping between the pure modal signal and PMU measurements using historical PMU measurement data; and (2) calculate the pure modal signal from PMU measurements using the identified mapping.

When the power oscillation occurs in the power grid, assume that there are total q oscillation modes. To proceed, let α_j, ω_j, and ϕ_j denote the damping ratio, angular oscillation frequency, and phase shift of the j-th oscillation mode, respectively. Then the j-th oscillation modal signal can be described as

$$
o_j(t) = e^{\alpha_j t} \cos\left(\omega_j t + \phi_j\right).
$$

On the other hand, let $f_i(t)$, $i = 1, \dots, m$, denote the i-th PMU measurement, where we assume that there are m PMUs in the system. It is also assumed that the number of PMUs is no less than that of the oscillation modes, that is, $m \geq q$. Then, the PMU measurements during oscillation can be approximately represented as the linear combination of those oscillation modal signals; that is,

$$
f_i(t) \approx \sum_{j=1}^{q} c_{ij} e^{\alpha_j t} \cos\left(\omega_j t + \phi_j\right) = \sum_{j=1}^{q} c_{ij} o_j(t), \tag{25}
$$

where c_{ij} represents the amplitude of the j-th oscillation modal signal in the i-th PMU measurement. For simplicity, (25) can be written in the vector form as $\boldsymbol{f}(t) = \boldsymbol{C}\boldsymbol{o}(t)$, where $\boldsymbol{f}(t) = \begin{bmatrix} f_1(t) & \cdots & f_m(t) \end{bmatrix}^{\mathrm{T}} \in \mathbb{R}^m$, $\boldsymbol{C} = \begin{bmatrix} c_{ij} \end{bmatrix} \in \mathbb{R}^{m \times q}$, and $\boldsymbol{o}(t) = \begin{bmatrix} o_1(t) & \cdots & o_q(t) \end{bmatrix}^{\mathrm{T}} \in \mathbb{R}^q$. Given PMU measurements in the past, we can apply the Prony's algorithm to determine the coefficient matrix $\boldsymbol{C}$. If $\boldsymbol{C}$ has left inverse denoted by $\boldsymbol{C}^{-L}$, then we can extract the dominant oscillation modal signals $\boldsymbol{o}(t)$ in real time as $\boldsymbol{o}(t) = \boldsymbol{C}^{-L}\boldsymbol{f}(t)$ when new PMU measurements are being received.

The extracted modal signals $o_j(t)$ can be used as the feedback signal to improve the damping of the j-th oscillation mode. Note that the coefficient matrix $\boldsymbol{C}$ depends on the system topology and operating point. Therefore, it is recommended that $\boldsymbol{C}$ be determined based on the PMU measurements after the oscillation to be damped.

5.3 Simulation Results

In this section, we consider the same minniWECC system as shown in Figure 15 to test the proposed rigorous approach of modal decomposition by implementing decoupled damping control over the PDCI. In the following simulation studies, the operating condition is selected such that the inter-area oscillation modes are shown in Table 3. A conventional power oscillation damping (POD) based on the frequency difference as defined by (14) was applied to the PDCI. The proposed decoupled controller is added as a supplementary controller to damp the BC mode with the frequency of 0.622 Hz. The performance of conventional POD with and without decoupled controller is tested and compared.

Table 3. Inter-area Oscillation Modes under Consideration for Decoupled Damping Control

Mode	Frequency (Hz)	Damping (%)
N-S	0.134	35.8
Alberta	0.292	3.1
E-W south 1	0.529	8.6
Montana	0.548	5.4
BC	0.622	1.0
E-W South 2	0.694	5.3
Middle	0.714	6.1

In the first scenario, a small disturbance is injected into the system to trigger the oscillation modes. Specifically, at time 1.0 second, a small pulse perturbation is added to the mechanical power of machine 10 at bus 24. The simulation results of oscillations observed in the AC power flow, bus voltage, and terminal frequency difference are shown in Figure 20. It can be seen that the supplementary decoupled method provides the best damping of the system—the oscillation magnitudes are dramatically decreased and the system returns to steady state much faster. The oscillations observed in machine speed and angle difference are shown in Figure 21. Similarly, with the proposed decoupled method, the system reaches the steady state much faster than with the conventional POD controller. A fast Fourier transform (FFT) analysis is also performed on the oscillation measurements where conventional POD controls are implemented with and without the supplementary decoupled method. The results are shown in Figure 22. The BC mode with 0.622 Hz frequency is precisely damped and the other modes remain almost unchanged. Again, the results confirm the precise damping capability of the proposed method.

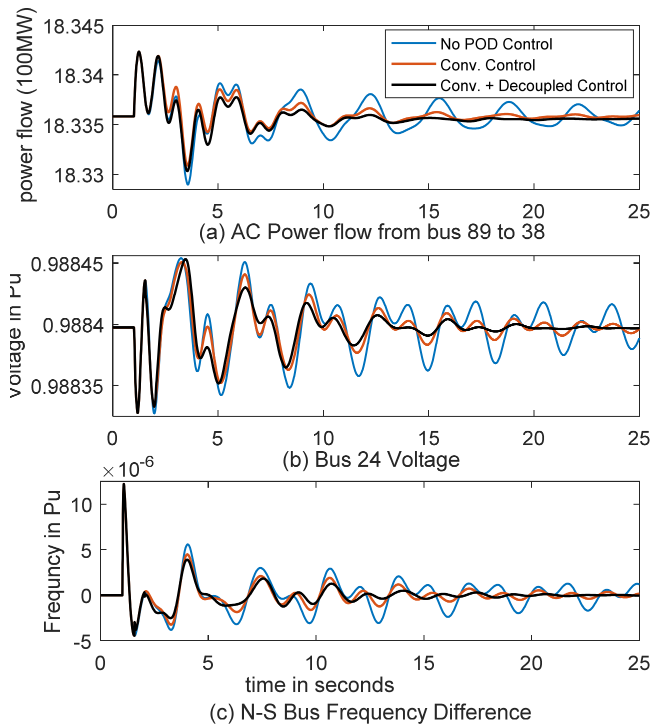

Figure 20. Comparison of POD Controllers with Respect to AC Power Flow, Bus Voltage, and Terminal Frequency Difference under the First Scenario

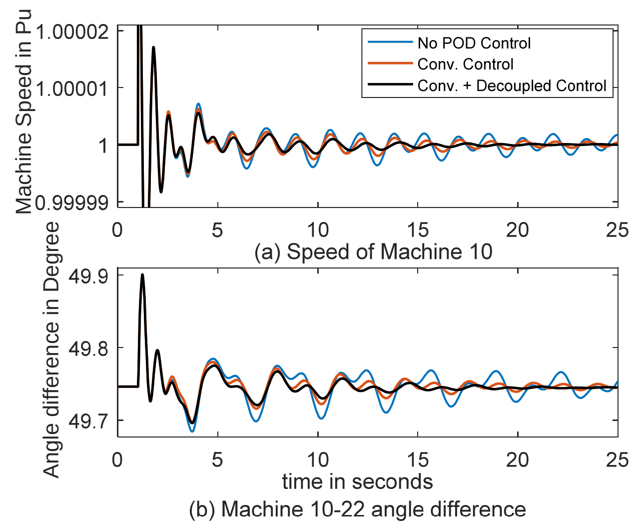

Figure 21. Comparison of POD Controllers with Respect to Machine Speed and Angle Difference under the First Scenario

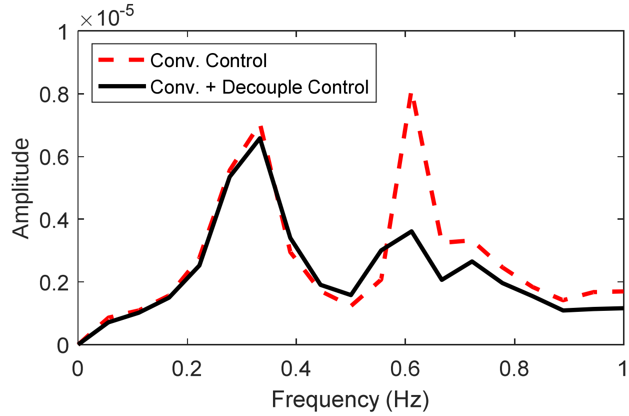

Figure 22. Frequency Analysis under the First Scenario

In the second scenario, a severe fault is applied to the system to test the performance of the proposed method under conditions of large disturbance. Specifically, at time 1.0 second, a three-phase fault occurs on the transmission line 86-87. The fault is cleaned one cycle later. Because the dynamics during the fault are much larger than the post-fault oscillations, all of the figures are magnified for better readability. The simulation results of oscillations observed in the AC power flow, bus voltage, and terminal frequency difference are shown in Figure 23 As seen in the figure, when the severe fault happens, the system experiences more drastic oscillations than it did in the first scenario. The supplementary decoupled method provides the best damping of the system—the oscillation magnitudes are dramatically decreased and the system returns to steady state much faster. The oscillations observed in machine speed and angle difference are shown in Figure 24. Similarly, with the proposed decoupled method, the system reaches steady state much faster than with the conventional POD controller. An FFT analysis of the oscillation measurements where conventional POD controls are implemented with and without the supplementary decoupled method is also performed for the second scenario. The results are shown in Figure 25. Similar to the first scenario, the BC mode with 0.622 Hz frequency is again precisely damped and the other modes remained almost unchanged. Again, the results of FFT analysis confirm the precise damping capability of the proposed method.

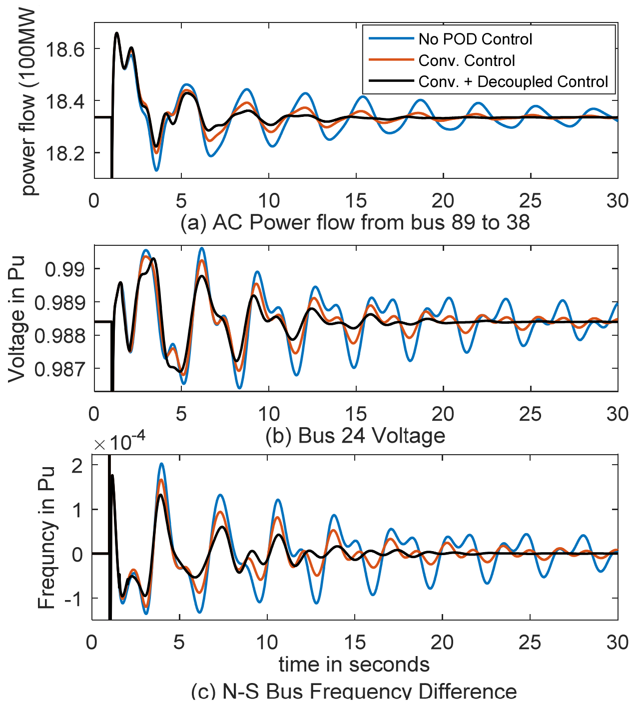

Figure 23. Comparison of POD Controllers with Respect to AC Power Flow, Bus Voltage, and Terminal Frequency Difference under the Second Scenario

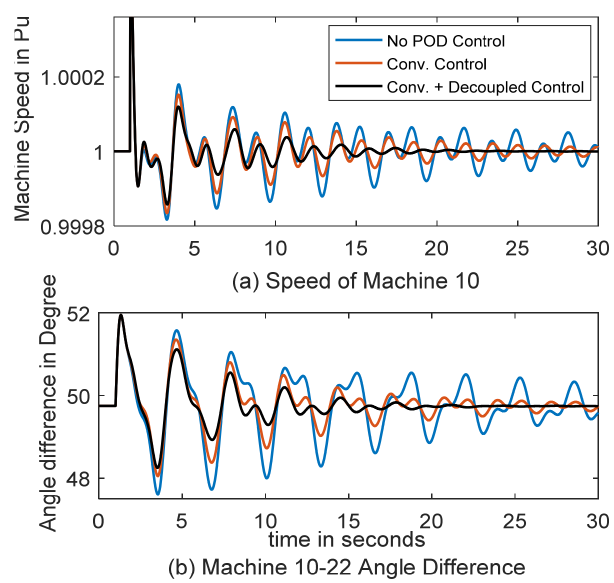

Figure 24. Comparison of POD Controllers with Respect to Machine Speed and Angle Difference under the Second Scenario

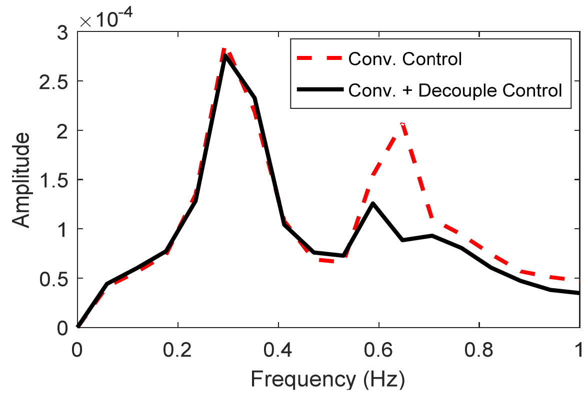

Figure 25. Frequency Analysis under the Second Scenario

6.0 Conclusions and Future Work

In this report, we developed a wide-area universal damping control to effectively mitigate inter-area oscillations in the power grid. The proposed damping control can be easily implemented by all kinds of fast-acting resources that are available in both transmission and distribution systems such as PSSs, FACTS devices, HVDC lines, and end-use devices. This feature greatly increases the applicability of the proposed damping control. Moreover, we proposed a rigorous method to extract pure oscillation modal signals from PMU measurements so that the decoupled damping control can be designed. With the proposed control methodology, we can manage the stability and reliability of the power grid in a much more flexible manner without being restricted by the resource availability. Moreover, we can achieve higher power transfer capacity by improving the damping of inter-area oscillations.

One of our next steps will be to investigate the impacts of communication effects (delay, packet loss, etc.) on damping control performance. Another step will be to improve the resilience of wide-area monitoring and control systems to cyber-physical attacks. These two problems are currently the most critical challenges facing any wide-area control strategies in the power grid.

7.0 Bibliography

Aboul-Ela, M. E., A. A. Sallam, J. D. McCalley, and A. A. Fouad (1996, May). Damping controller design for power system oscillations using global signals. *IEEE Transactions on Power Systems 11*(2), 767–773.

Bertsch, J., C. Carnal, D. Karlsson, J. Mcdaniel, and K. Vu (2005, May). Wide-area protection and power system utilization. *Proc. IEEE 93*(5), 997–1003.

Borovikov, Y. S., A. S. Gusev, A. O. Sulaymanov, R. A. Ufa, A. S. Vasilev, M. V. Andreev, N. Y. Ruban, and A. A. Suvorov (2016, Sept). A hybrid simulation model for VSC HVDC. *IEEE Transactions on Smart Grid 7*(5), 2242–2249.

Callaway, D. S. and I. A. Hiskens (2011, January). Achieving controllability of electric loads. *Proc. IEEE 99*(1), 184–199.

Cresap, R. L. and W. A. Mittelstadt (1976, Mar). Small-signal modulation of the Pacific HVDC Intertie. *IEEE Transactions on Power Apparatus and Systems 95*(2), 536–541.

Cresap, R. L., W. A. Mittelstadt, D. N. Scott, and C. W. Taylor (1978, July). Operating experience with modulation of the Pacific HVDC Intertie. *IEEE Transactions on Power Apparatus and Systems PAS-97*(4), 1053–1059.

Dougherty, J. and T. Hillesland (1970). Power system stability considerations with dynamically responsive DC transmission lines. *IEEE Transactions on Power Apparatus and Systems PAS-89*(1), 34–45.

El-Moursi, M. S., B. Bak-Jensen, and M. H. Abdel-Rahman (2010, February). Novel STATCOM controller for mitigating SSR and damping power system oscillations in a series compensated wind park. *IEEE Transactions on Power Electronics 25*(2), 40–45.

Etingov, P., F. Tuffner, J. Follum, Z. Hou, D. Kosterev, G. Matthews, and B. Lesieutre (2017). *Oscillation baselining and analysis tool*. Salt Lake City.

Farsangi, M. M., Y. H. Song, and K. Y. Lee (2004, May). Choice of FACTS device control inputs for damping interarea oscillations. *IEEE Transactions on Power Systems 19*(2), 1135–1143.

Gibbard, M. J., D. J. Vowles, and P. Pourbeik (2000, May). Interactions between, and effectiveness of, power system stabilizers and FACTS devices stabilizers in multimachine systems. *IEEE Transactions on Power Systems 15*(2), 748–755.

Harley, R. G. and J. C. Balda (1985, May). Subsynchronous resonance damping by specially controlling a parallel HVDC link. *IEE Proceedings C - Generation, Transmission and Distribution 132*(3), 154–160.

Harnefors, L., N. Johansson, L. Zhang, and B. Berggren (2014, Sept). Interarea oscillation damping using active-power modulation of multiterminal HVDC transmissions. *IEEE Transactions on Power Systems 29*(5), 2529–2538.

Huang, Z., N. Zhou, F. Tuffner, Y. Chen, D. J. Trudnowski, W. Mittelstadt, J. Hauer, and J. Dagle (2010, July). Improving small signal stability through operating point adjustment. In *Proc. 2010 IEEE PES General Meeting*, Minneapolis, MN.

Kamwa, I., R. Grondin, and Y. Hébert (2001, February). Wide-area measurement based stabilizing control of large power systems–A decentralized/hierarchical approach. *IEEE Transactions on Power Systems 16*(1), 136–153.

Klein, M., G. J. Rogers, and P. Kundur (1991). A fundamental study of inter-area oscillations in power systems. *IEEE Transactions on Power Systems 6*(3), 914–920.

Kosterev, D. N., C. W. Taylor, and W. A. Mittelstadt (1999, August). Model validation for the August 10, 1996 WSCC system outage. *IEEE Transactions on Power Systems 14*(3), 967–979.

Kundur, P. (1994). *Power system stability and control*. New York: McGraw-Hill.

Lerch, E., D. Povh, and L. Xu (1991, May). Advanced SVC control for damping power system oscillations. *IEEE Transactions on Power Systems 6*(2), 524–535.

Li, Y., C. Rehtanz, S. Rüberg, L. Luo, and Y. Cao (2012, July). Wide-area robust coordination approach of HVDC and FACTS controllers for damping multiple interarea oscillations. *IEEE Transactions on Power Delivery 27*(3), 1096–1105.

Lian, J., J. Hansen, L. D. Marinovici, and K. Kalsi (2016, July). Hierarchical decentralized control strategy for demand-side primary frequency response. In *Proc. 2016 IEEE PES General Meeting*, pp. 1–5.

Mithulananthan, N., C. A. Canizares, J. Reeve, and G. J. Rogers (2003, May). Comparison of PSS, SVC, and STATCOM controllers for damping power system oscillations. *IEEE Transactions on Power Systems 18*(2), 786–792.

Motalleb, M., M. Thornton, E. Reihani, and R. Ghorbani (2016). Providing frequency regulation reserve services using demand response scheduling. *Energy Conversion and Management 124*, 439 – 452.

Neely, J. C., R. H. Byrne, R. T. Elliott, C. A. Silva-Monroy, D. A. Schoenwald, D. J. Trudnowski, and M. K. Donnelly (2013, July). Damping of inter-area oscillations using energy storage. In *Proc. 2013 IEEE PES General Meeting*, Vancouver, BC.

Ni, Y. X. and A. A. Fouad (1987, Nov). A simplified two-terminal HVDC model and its use in direct transient stability assessment. *IEEE Transactions on Power Systems 2*(4), 1006–1012.

Pal, B. C., A. H. Coonick, and D. C. Macdonald (2000, February). Robust damping controller design in power systems with superconducting magnetic energy storage devices. *IEEE Transactions on Power Systems 15*(1), 320–325.

Pierre, B., R. Elliott, D. Schoenwald, J. Neely, R. Byrne, D. Trudnowski, and J. Colwell (2016, July). Supervisory system for a wide area damping controller using PDCI modulation and real-time PMU feedback. In *Proc. 2016 IEEE PES General Meeting*, pp. 1–5.

Pipelzadeh, Y., B. Chaudhuri, and T. C. Green (2010, July). Wide-area power oscillation damping control through HVDC: A case study on Australian equivalent system. In *Proc. IEEE PES General Meeting*, pp. 1–7.

Piwko, R. J. and E. V. Larsen (1982, July). HVDC system control for damping of subsynchronous oscillations. *IEEE Transactions on Power Apparatus and Systems PAS-101*(7), 2203–2211.

Schoenwald, D. A., B. J. Pierre, F. Wilches-Bernal, and D. J. Trudnowski (2017, July). Design and implementation of a wide-area damping controller using high voltage DC modulation and synchrophasor feedback. In *Proc. the 20th World Congress of the International Federation of Automatic Control*, Toulouse, France.

Trudnowski, D. (2008, September). The MinniWECC System Model. Appendix 2 of Year 1 report of BPA contract 37508.

Trudnowski, D. J., D. Kosterev, and J. Undrill (2013, July). PDCI damping control analysis for the western North American Power System. In *Proc. 2013 IEEE PES General Meeting*, Vancouver, BC.

Yang, N., Q. Liu, and J. McCalley (1998, November). TCSC controller design for damping interarea oscillations. *IEEE Transactions on Power Systems 13*(4), 1304–1310.

Zarghami, M., M. L. Crow, J. Sarangapani, Y. Liu, and S. Atcitty (2010, February). A novel approach to interarea oscillation damping by unified power flow controllers utilizing ultracapacitors. *IEEE Transactions on Power Systems 25*(1), 404–412.

Zhang, J., C. Y. Chung, and Y. Han (2012, November). A novel modal decomposition control and its application to PSS design for damping interarea oscillations in power systems. *IEEE Transactions on Power Systems 27*(4), 2015–2025.

Zhang, Y. and A. Bose (2008, August). Design of wide-area damping controllers for interarea oscillations. *IEEE Transactions on Power Systems 23*(3), 1136–1143.

Zhou, H., G. Yang, and J. Wang (2011, March). Modeling, analysis, and control for the rectifier of hybrid HVdc systems for DFIG-based wind farms. *IEEE Transactions on Energy Conversion 26*(1), 340–353.

Distribution

No. of Copies		No. of Copies	
1	U.S. Department of Energy 1000 Independence Avenue, SW Washington, DC 20585 Phil N. Overholt	2	**Local Distribution** Pacific Northwest National Laboratory Eric Andersen J4-90 Dale King K6-05

Pacific Northwest
NATIONAL LABORATORY

U.S. DEPARTMENT OF
ENERGY

Proudly Operated by **Battelle** *Since 1965*

902 Battelle Boulevard
P.O. Box 999
Richland, WA 99352
1-888-375-PNNL (7665)

www.pnnl.gov